Extending the capabilities of the dual-grid finite-difference time-domain method

Romain Pascaud[1], Gaël Godi[1], Raphaël Gillard[1], Renaud Loison[1], Joe Wiart[2] and Man-Faï Wong[2]

Abstract – In this paper, improvements of the dual-grid finite-difference time-domain (DG-FDTD) method are proposed. This multiresolution approach is particularly suitable for the simulation of surrounded antenna problems. By successively combining two finite-difference time-domain (FDTD) simulations with different resolutions, it allows the evaluation of the environment effects on the radiated fields, and it also gives information on the antenna input impedance. In this paper, we propose two different techniques to extend the DG-FDTD capabilities. The first one consists of a correction procedure. Its application to a lens antenna analysis exhibits accurate results while providing a computation speedup of 16.7. The second technique consists of its hybridization with the multiple-region FDTD to make the simulation of transmission problems possible. A study involving two ultra-wide band antennas shows the relevance of the hybrid method that allows a fast and accurate characterization of scattering parameters.

Index Terms – FDTD methods, Numerical analysis, Lens antennas, Antenna array mutual coupling.

I. Introduction

Although the finite-difference time-domain (FDTD) method [1] is a powerful, robust, and popular tool for the analysis of various structures over a large bandwidth, the simulation of large problems such as large antennas or antenna arrays remains a current issue. Actually, the antenna often requires a fine description to deal with near-field parameters like the impedance, whereas its environment does not need such a discretization. The uniform discretization of the classical FDTD volume finally leads to oversampled areas that increases the computational time.

Nonuniform orthogonal grids or graded mesh are common solutions to deal with the discretization problem [2]. However, these methods are limited to specific geometries that conform to the specialized grid.

A multiresolution time-domain (MRTD) approach has been introduced as an alternative to classical FDTD [3]. It uses a wavelet expansion of the fields in the FDTD volume, and the vanishing moments properties of wavelet, to reduce the computational requirements. Nonetheless, the MRTD can be cumbersome when boundary conditions are involved. Moreover, no actual thresholding criterion exists that allows an automated choice of the wavelet components to be neglected.

The multiple-region finite-difference time-domain (MR-FDTD) approach has been proposed for the simulation of problems where distant elements are involved in an infinite homogeneous medium [4]. The MR-FDTD divides the classical FDTD volume into sub-volumes that interact with each other thanks to radiation integrals. Significant savings can be made since there is no need to mesh the space between the sub-volumes. It also reduces the numerical dispersion involved in large meshed regions. However, compression techniques are required to make the MR-FDTD competitive with the classical FDTD in terms of computational time [5]. Unfortunately, it generates an instability during the calculation. One way to overcome this instability issue is to consider an unilateral MR-FDTD instead of a bilateral one [6]. Nevertheless, it may be inaccurate if the sub-volumes are close since the second-order coupling effects are not taken into account.

Subgridding finite-difference time-domain (SG-FDTD) schemes have also been intensively investigated [7-12]. Various approaches exist: sequential computations [7], subgridding in space only [8], and subgridding in space and time [9-12]. Whatever the subgridding technique, it always consists in using different cell sizes over different areas of the volume. During the simulation, the fields on the boundary of one grid are used to compute the fields on the boundary of the other grid. Nevertheless, spurious reflections from the interface exist that limit the ratio of spatial steps between the grids [9-11]. Moreover, a late time instability may appear when computing the electromagnetic fields [12].

Recently, the dual-grid finite-difference time-domain (DG-FDTD) approach has been introduced by the authors for the fast simulation of surrounded antennas [13]. The DG-FDTD successively combines two FDTD simulations with different resolutions. Firstly, the antenna is characterized without its environment using a fine FDTD simulation. Secondly, the surrounded performance of the antenna are evaluated using a coarse FDTD simulation of the antenna with its environment. Therefore, the DG-FDTD is particularly suitable to compute the environment effects on the radiated fields [13, 14]. It also gives the modifications on the input impedance of the antenna due to the environment.

Since these modifications are computed with a coarse FDTD, we only have an approximate value of the modified impedance. We proposed in this paper a correction procedure to improve the computation of the surrounded

impedance. A second critical situation can be encountered when we try to extend the DG-FDTD to transmission problems. In this case, the coarse description of the environment, that includes the receiving structure, does not lead to an accurate transmission coefficient. We then propose to hybridize the DG-FDTD with the unilateral MR-FDTD to analyze such a transmission problem [15].
The discussion proceeds with a reminder of the DG-FDTD principle in Section II. Section III presents a new possible application of the DG-FDTD: the fast and accurate simulation of lens antennas. The correction procedure is then described and applied to this test case. Afterwards, the hybridization of the DG-FDTD with the unilateral MR-FDTD is detailed in Section IV. Finally, some conclusions are drawn in Section V.

II. DG-FDTD method

A) DG-FDTD principle

Consider the open problem presented in Figure 1(a), where an antenna is placed near a scattering element. As shown in Figure 1(b), the DG-FDTD simulation divides the overall analysis into two different FDTD simulations.

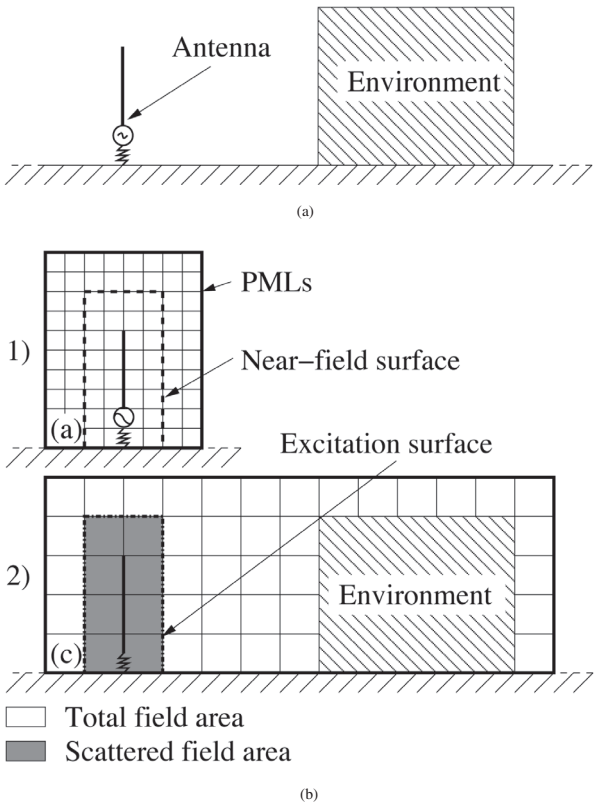

Fig. 1. (a) Electromagnetic problem, (b) DG-FDTD decomposition.

Firstly, we define a finely discretized FDTD volume that only includes the antenna. This FDTD volume is terminated by perfectly matched layers (PMLs) in order to simulate an infinite problem [16]. This simulation goes from t_0 to $T_{obs_{\text{fine}}}$ with a time step $d_{t_{\text{fine}}}$ that respects the Courant-Friedrich-Levy (CFL) stability condition. $T_{obs_{\text{fine}}}$ is chosen so that the electromagnetic energy may be radiated outside the FDTD volume. We finally have the characteristics of the antenna without its environment. During this simulation, the "primary" radiation of the antenna, namely when no disturbing environment is involved, is stored on a near-field surface. Such a radiation is calculated with a good accuracy thanks to the fine discretization.
Secondly, this primary radiation is used as the excitation of a coarse FDTD simulation that represents both the antenna and its environment. The excitation is carried out by means of an excitation surface based on the total field/scattered field decomposition principle [17]. This simulation also starts at t_0, but ends at $T_{obs_{\text{coarse}}}$ which can be larger than $T_{obs_{\text{fine}}}$, depending on the size of the problem. The time step $d_{t_{\text{coarse}}}$ used in the second simulation might be larger than $d_{t_{\text{fine}}}$ since the spatial steps, and thus the CFL condition, are different. Note that a coarse description of the antenna is included to deal with second-order scattering phenomena. It guarantees that all coupling effects between the antenna and its environment are taken into account, and especially the influence of the backscattered field on the antenna input impedance. Besides, the generator of the antenna has to be switched off since the incident power is already present in the primary radiation that is used as the excitation of the coarse FDTD volume. This second step may be combined with a correction procedure that is presented in details in Section III.D.
To sum up, the DG-FDTD enables the computation of the surrounded characteristics of the antenna in a fast way, but it also makes possible the accurate simulation of the antenna without its environment. The DG-FDTD turns out to be well adapted to problems that imply a lot of simulations where the environment is changed. Indeed, once the antenna is characterized with the fine FDTD, it can be quickly simulated in various configurations thanks to the coarse FDTD. The DG-FDTD remains stable since it combines two classical FDTD simulations that both respect their own CFL stability condition. Furthermore, it is easy to implement in contrast with other FDTD multiresolution approaches. Actually, only the excitation mechanism must be added to a classical FDTD code.

B) DG-FDTD post-processings

The DG-FDTD method allows the evaluation of the antenna characteristics with and without its environment. In order to compute both the different reflection parameters, we use

$$S_{11}(f) = \frac{b_1(f)}{a_1(f)} \tag{1}$$

where S_{11} is the reflection parameter, whereas a_1 and b_1 are the incident and reflected waves at the generator terminals, respectively. Actually, the reflected wave b_1 can

be divided into two waves: the one due to the antenna, and the one due to the environment. Hence, it is possible to compute the reflection parameter without the environment by considering $b_1 = b_{1_{\text{fine}}}$, where $b_{1_{\text{fine}}}$ is calculated during the first step of the DG-FDTD. On the other hand, the S_{11} parameter with the environment requires to add the reflected waves coming from both FDTD simulations: $b_1 = b_{1_{\text{fine}}} + b_{1_{\text{coarse}}}$.
The radiation patterns are calculated by means of a near-to-far-field transformation based on the Huygens principle [18]. A Huygens surface is defined in the FDTD volume, and the field components on this surface are stored at each time step. Once the simulation is over, the electric and magnetic equivalent currents ($\vec{J}$ and $\vec{M}$) are evaluated in the frequency domain. Finally, the far-fields are computed with a near-to-far-field transformation in the frequency domain that involves a numerical integration of the equivalent currents. The radiation patterns of the antenna are obtained by considering a Huygens surface that totaly includes the antenna in the first step of the DG-FDTD simulation. With regard to the far-field of the overall problem, it is calculated using a Huygens surface that includes both the antenna and its environment during the second step of the DG-FDTD simulation.

III. Simulation of integrated lens antennas using the DG-FDTD

A) Integrated lens antennas

The significant increase of millimeter-wave applications in the last decades is partially explained by the congestion of the frequency spectrum. As a result, antenna designers have to focus on millimeter-wave antenna design and optimization. Among the variety of millimeter-wave antennas, integrated lens antennas (ILA) are widely spread [19-22]. An ILA consists of a dielectric lens fed by a primary source in direct contact with the lens body. Depending on the required radiation characteristics, the lens radius may be equal to several wavelengths. In order to simulate such an electrically large antenna, asymptotic methods are often used since they are efficient from the calculation point of view [19, 20]. However, they still suffer from inaccuracies since the multiple internal reflections are not well taken into account [21]. A fullwave electromagnetic method is needed to perform fully accurate simulation of the ILA.
FDTD technique has already been successfully applied to the analysis of three-dimensional lenses [21, 22]. Nonetheless, the uniform discretization of the classical FDTD may be a problem. Actually, the source often requires a fine discretization to deal with short dimensions, whereas the lens shape does not. The uniform small spatial steps finally lead to huge computational time and memory requirements. We propose to analyze integrated lens antennas with the DG-FDTD method.

B) DG-FDTD simulation of integrated lens antennas

As mentioned in Section II.A, the DG-FDTD involves two FDTD simulations with different resolutions (Fig. 2).

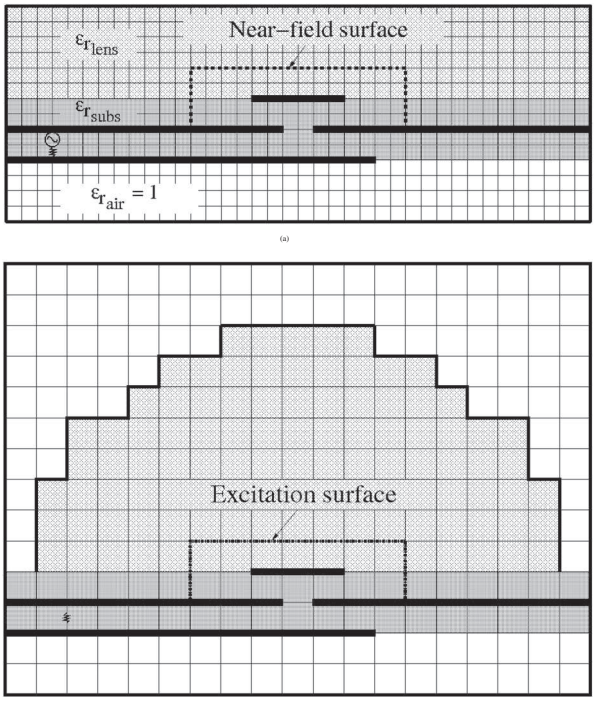

Fig. 2. DG-FDTD application to the ILA analysis: (a) fine FDTD simulation of the primary source, (b) coarse FDTD simulation of the overall structure.

The primary source is firstly simulated alone while storing its primary radiation on a near-field surface (Fig. 2(a)). The FDTD volume is terminated by uniaxial PMLs [23] to simulate an infinite problem. As a result, the primary source radiates in an infinite dielectric medium with $\epsilon_{r_{\text{lens}}}$. Secondly, the primary radiation of the source is used to excite a coarse FDTD volume that represents both the source and the dielectric lens (Fig. 2(b)). The presence of the primary source in the coarse simulation guarantees that the multiple internal reflections are taken into account to compute the S_{11} parameter. One may note that Figure 2 is a schematic, and in practical the lens is several wavelengths when the primary source is very small.

C) Numerical example

The simulated integrated lens antenna is presented in Figure 3. This axisymmetric ILA has been designed and optimized in [20] to provide a sectoral shaped coverage. Its diameter and height are equal to $6.1 \times \lambda_0$ and $4.1 \times \lambda_0$ ($f_0 = 28$ GHz), respectively. The primary source and lens characteristics are presented in [20].
In order to evaluate the accuracy of the DG-FDTD, three approaches are compared (Table 1). The classical fine FDTD involves small spatial steps: $dx_{\text{fine}} = dy_{\text{fine}} = \lambda_0/102$, and $dz_{\text{fine}} = \lambda_0/84$ at $f_0 = 28$ GHz. It enables us to deal with short dimensions of the primary source.

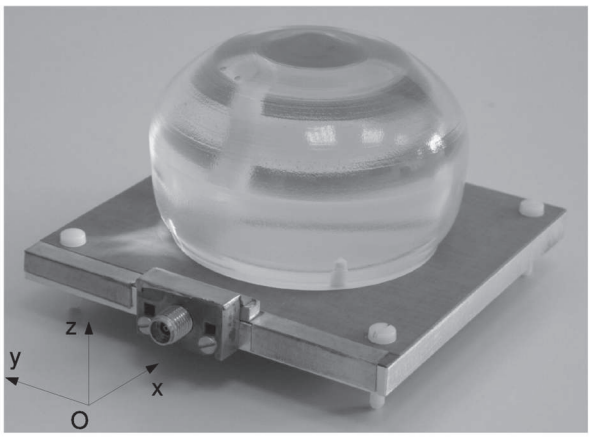

Fig. 3. Simulated axisymmetric ILA.

On the opposite, the classical coarse FDTD compels us to make some approximations. In this particular case, the spatial steps dx_{coarse} and dy_{coarse} are three times larger, and dz_{coarse} is twice larger, than those of the fine FDTD ($dx_{\text{coarse}} = dy_{\text{coarse}} = \lambda_0/34$, and $dz_{\text{coarse}} = \lambda_0/42$). Concerning the DG-FDTD, the primary source is simulated alone using the fine discretization, whereas the second simulation involves the coarse description of the entire structure.

Figure 4(a) presents the simulated far-field radiation patterns in the (yOz) plane at $f_0 = 28$ GHz. The DG-FDTD and the classical coarse FDTD results are in good agreement with the classical fine FDTD results. Both main lobe and sidelobes are well predicted by those methods. Actually, the coarse mesh resolution is accurate enough to analyze the far-field.

The simulated reflection parameters are reported in Figure 4(b). We first notice that the reflection parameter depends on the presence of the lens. Indeed, some rippling effects appear in the $|S_{11}|$ parameter. Concerning the coarse classical FDTD, the reflection parameter turns out to be inaccurate. The response is shifted in frequency, and the bandwidth at -10 dB is over-evaluated. Concerning the DG-FDTD, the response is better, and the ILA bandwidth is well predicted. Some rippling effects due to the dielectric lens are observed. Nevertheless, there is still several differences. In fact, the primary source in the coarse simulation is not matched at all at $f_0 = 28$ GHz since its response is shifted in frequency by 3.5 GHz. Hence, for highly resonant structures, the coarse representation of the source might lead to inaccuracies on the reflection parameter. In the next Section, a correction procedure is proposed to deal with this problem.

As far as computing time and memory requirements are concerned, the fine FDTD simulation of the ILA requires 104 hours and 7500 MB using an AMD 64-4200 PC. The coarse FDTD simulation only needs 4 hours and 21 minutes, and 627 MB. The DG-FDTD simulation takes 6 hours and 13 minutes: 1 hour and 52 minutes for the first step, and 4 hours and 21 minutes for the second step. Concerning the memory requirements, they are 74 MB for the first step, and 627 MB for the second one. Finally, we have a computational speedup of 16.7, and a reduction by 10.7 of the memory requirements.

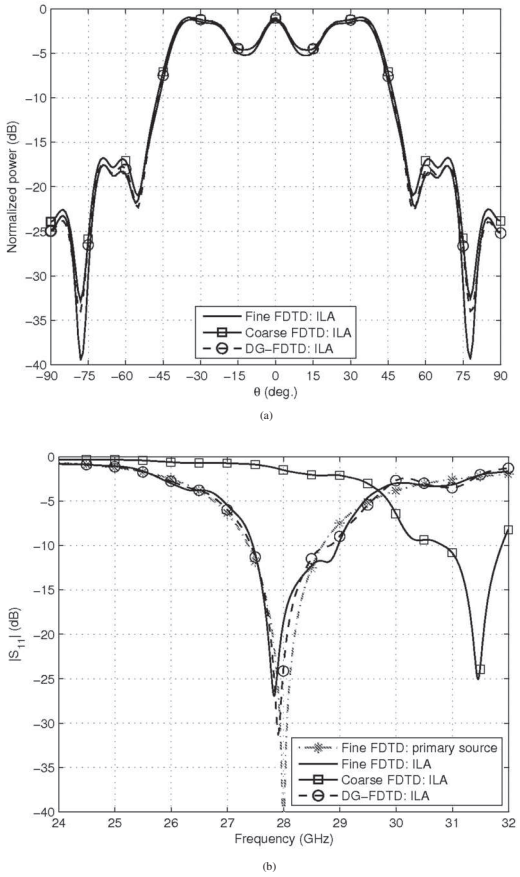

Fig. 4. Simulation results: (a) far-field radiation patterns in the (yOz) plane at $f_0 = 28$ GHz, (b) $|S_{11}|$.

D) Correction procedure

As we have seen in Section III.C, some differences are observed between the reflection parameters obtained with the DG-FDTD and the fine FDTD (Fig. 4(b)). The coarse discretization of the primary source during the second step of the DG-FDTD leads to an inaccurate reflected wave $b_{1_{\text{coarse}}}$. A simple correction procedure can be carried out to improve the evaluation of the reflection parameter (Fig. 5). This correction procedure requires a coarse simulation of the primary source alone in addition to the two FDTD simulations involved in the DG-FDTD (Fig. 5(b)). Two field components are stored by means of probes in each FDTD simulation of the primary source. Two transfer functions T are evaluated by calculating

$$T_{\text{fine}}(f) = \frac{E_{x_{\text{fine}}}(f)}{E_{z_{\text{fine}}}(f)} \tag{2}$$

and

$$T_{\text{coarse}}(f) = \frac{E_{x_{\text{coarse}}}(f)}{E_{z_{\text{coarse}}}(f)} \tag{3}$$

	Fine FDTD	Coarse FDTD	DG-FDTD	
			First step	Second step
Spatial steps: $dx = dy$	0.105 mm	0.315 mm	0.105 mm	0.315 mm
Spatial step: dz	0.127 mm	0.254 mm	0.127 mm	0.254 mm
Volume size: $N_x \times N_y \times N_z$	$673 \times 673 \times 397$	$253 \times 253 \times 212$	$151 \times 151 \times 57$	$253 \times 253 \times 212$
Time step: dt	0.2 ps	0.53 ps	0.2 ps	0.53 ps
Observation time: T_{obs}	3 ns	3 ns	3 ns	3 ns
Near-field surface: $N_x \times N_y \times N_z$	-	-	$117 \times 117 \times 36$	-
Excitation surface: $N_x \times N_y \times N_z$	-	-	-	$39 \times 39 \times 18$

Table 1. Different simulation approaches: parameters.

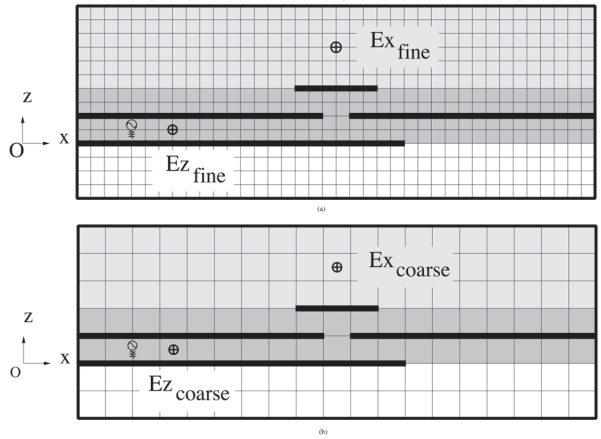

Fig. 5. Correction procedure for the DG-FDTD method: (a) fine FDTD simulation of the primary source, (b) coarse FDTD simulation of the primary source.

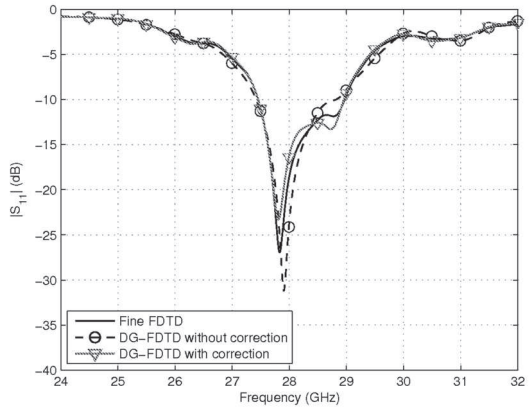

Fig. 6. Simulated $|S_{11}|$ as a function of the frequency for the DG-FDTD with and without correction.

where E_z is the incident field component in the microstrip line of the primary source, whereas E_x is the major field component radiated by the primary source inside the dielectric media. These transfer functions give an information of the fine and coarse transmission between the generator and the direction of maximum radiating in the homogeneous dielectric media. Note that each component is taken at the same physical position in the fine and coarse simulations.

The inaccurate reflected wave $b_{1_{\text{coarse}}}$ is finally corrected during the computation of the surrounded S_{11} parameter using

$$S_{11}(f) = \frac{b_{1_{\text{fine}}}(f) + b_{1_{\text{coarse}}}(f).\frac{T_{\text{fine}}(f)}{T_{\text{coarse}}(f)}}{a_1(f)}. \quad (4)$$

As we can see in Figure 6, the correction procedure improves the accuracy of the DG-FDTD method.

The correction procedure involves a coarse simulation of the primary source that requires 8 minutes, namely 2.1 % of the overall computational time. The DG-FDTD with the correction procedure turns out to be a good approach to simulate lens antennas.

IV. Hybridization of MR-FDTD and DG-FDTD methods

Section III has shown that the DG-FDTD accuracy might suffer from the coarse description of the primary source during the second step of the simulation. In the same way, the dual-grid FDTD approach may be inaccurate if both the antenna and the environment require a fine discretization. Consequently, the analysis of transmission between antennas remains a problem using the DG-FDTD method. We propose in this Section to hybridize the DG-FDTD with the unilateral MR-FDTD to analyze the transmission between antennas.

A) Test case

Figure 7 presents the problem to be simulated. It consists of two ultra wide-band (UWB) monopole antennas [24] placed on an infinite ground plane, and separated by D. Antenna 1 is fed with a matched generator that produces a time domain Gaussian pulse, narrow enough to cover the studied bandwidth (from 0 to 14 GHz). Antenna 2 acts as a matched antenna.

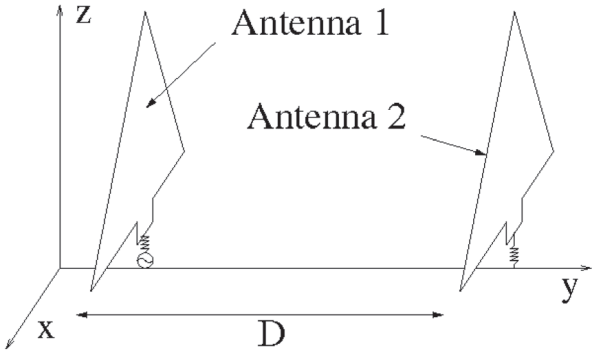

Fig. 7. Simulated test case: coupling between two UWB antennas.

The triangle-shaped geometry of the antennas implies a fine spatial discretization that leads to an oversampled FDTD volume. Thus, various advanced approaches are considered: DG-FDTD, unilateral MR-FDTD, and the proposed hybrid approach based on the unilateral MR-FDTD and the DG-FDTD. During this study, two spatial discretization are considered: a fine one with $dx_{\text{fine}} = dy_{\text{fine}} = dz_{\text{fine}} = 0.3$ mm $= \lambda_0/140$, and a coarse one with $dx_{\text{coarse}} = dy_{\text{coarse}} = dz_{\text{coarse}} = 1.2$ mm $= \lambda_0/35$ ($f_0 = 7$ GHz).

B) Unilateral MR-FDTD principle

The unilateral multiple-region FDTD is depicted in Figure 8(a). In this example, two sub-volumes are involved: sub-volume (a) that includes antenna 1, and sub-volume (b) that contains antenna 2. Firstly, antenna 1 is simulated alone in sub-volume (a) while storing the field in the near-field surface at each time step. Thus, we determine and store the primary radiation of antenna 1, that is to say its radiation when no disturbing environment is involved. Secondly, this stored field is used to excite sub-volume (b) by means of the radiation integrals. Note that it is possible to evaluate various configurations of the environment without simulating again antenna 1.
The unilateral MR-FDTD differs from the classical bilateral one by neglecting the feedback from antenna 2 to antenna 1. Hence, the inherent instability of the bilateral MR-FDTD is avoided, while still enabling the direct transmission to be finely characterized. However, it can lead to inaccuracies on the antenna 1 reflection parameter since the backscattered field from antenna 2 to antenna 1 is not taken into account.
In our case, sub-volumes (a) and (b) are finely discretized with $88 \times 40 \times 80$ cells, and compression techniques are involved to reduce the computational time of Kirchhoff integrals [5].
Figure 8(b) presents the hybrid approach based on the unilateral MR-FDTD and the DG-FDTD.
The MR-FDTD/DG-FDTD approach is divided into three steps. Firstly, we simulate antenna 1 alone in sub-volume (a), while storing its primary radiation in the near-field surface 1. Secondly, this stored field is radiated to-

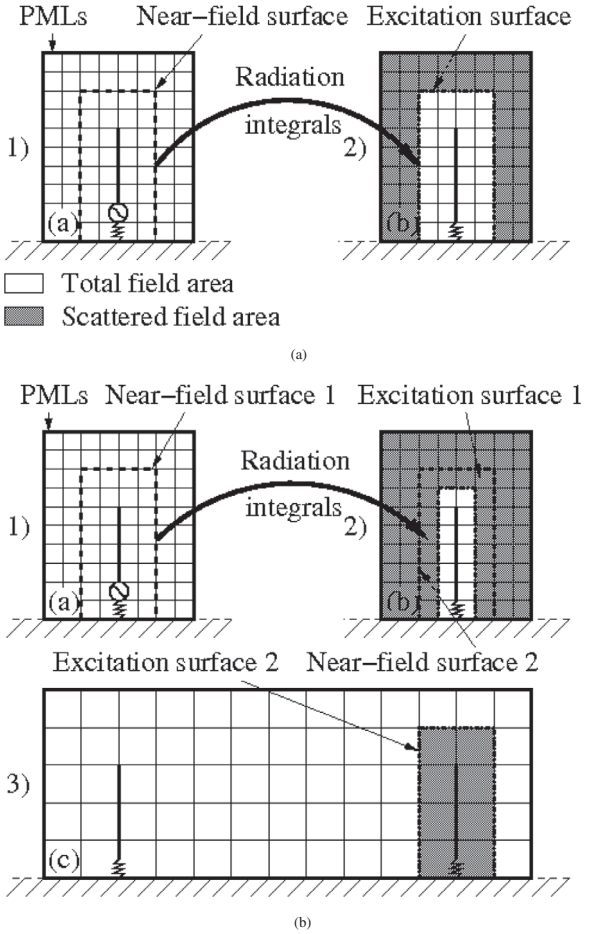

Fig. 8. Advanced FDTD methods decomposition: (a) unilateral MR-FDTD, (b) MR-FDTD/DG-FDTD.

wards antenna 2 thanks to the radiation integrals. During the second step, the near-field surface 2 is implemented in sub-volume (b), in order to store the field scattered by antenna 2. Finally, this stored field is used as the excitation of the coarse FDTD volume (c) that includes the overall structure. In fact, the first two steps consist of a unilateral MR-FDTD simulation, whereas the third step is a DG-FDTD simulation. The correction procedure presented in Section III.D might also be applied, but in this example the coarse description of antenna 1 is accurate enough to take into account the second order coupling effects.
Sub-volumes (a) and (b) are both finely discretized with $88 \times 40 \times 80$ cells, and compression techniques are still involved. Sub-volume (c) uses the $\lambda_0/35$ mesh. The size of this volume depends on the distance D between the antennas.

C) Numerical results

The accuracy of the MR-FDTD/DG-FDTD approach is now evaluated. A parametric study is performed considering the test case shown in Figure 7.
Table 2 presents the involved FDTD volumes as well as their associated mesh densities for the five simulation ap-

proaches that are considered. The classical FDTD simulations use uniform cubic mesh.

The S parameters derived from each simulation are compared with the reference ones by evaluating the mean squared difference ϵ_{ij} given by

$$\epsilon_{ij} = \sqrt{\frac{1}{N_f} \sum_{f=f_{\min}}^{f_{\max}} ||\mathrm{S}_{ij\mathrm{Ref}}(f)| - |\mathrm{S}_{ij}(f)||^2} \quad (5)$$

where N_f is the number of frequency points, Ref is for Reference, $f_{\min}$ is equal to 0 GHz, $f_{\max}$ is equal to 14 GHz, and S_{ij} is a linear value.

Figure 9 shows the error ϵ_{11} and ϵ_{21} as a function of the simulation approach and the distance D that ranges from 9.6 to 96 mm.

- The classical coarse FDTD turns out to be inaccurate whatever the distance D. The important error is due to the coarse description of the antenna geometry.
- The DG-FDTD gives good results for the $|\mathrm{S}_{11}|$ (especially if $D > 25$ mm). Indeed, the main part of the reflection is firstly simulated with a fine FDTD, and combined with a coarse evaluation of the backscattered field due to antenna 2. On the contrary, the DG-FDTD gives poor results for $|\mathrm{S}_{21}|$. This is due to the coarse discretization of antenna 2 during the second step of the DG-FDTD.
- The unilateral MR-FDTD exhibits inaccuracies on the S parameters for short distances (until 40 mm). The sizeable second-order coupling effects are not taken into account with this approach.
- The hybrid method turns out to be accurate on the S parameters for a large range of distances. The hybridization of the unilateral MR-FDTD and the DG-FDTD takes advantage of both methods.

Figure 10(a) presents the computational time as a function of the distance D. The coarse FDTD and the DG-FDTD are always faster than the fine FDTD, whereas the unilateral MR-FDTD and the hybrid approach become competitive when $D > 15$ mm.

Figure 10(b) exhibits the cumulative calculation time. The simulation of a given distance D between antennas with classical FDTD requires the simulation of the overall structure. As a result, if we consider N different distances, we need to simulate N large FDTD volumes. For the multiresolution approaches, it is different. We only require one fine simulation of antenna 1. Once antenna 1 is characterized, we just need to perform the further simulations for each distance, namely a coarse simulation of the overall structure for the DG-FDTD, a fine simulation of an-

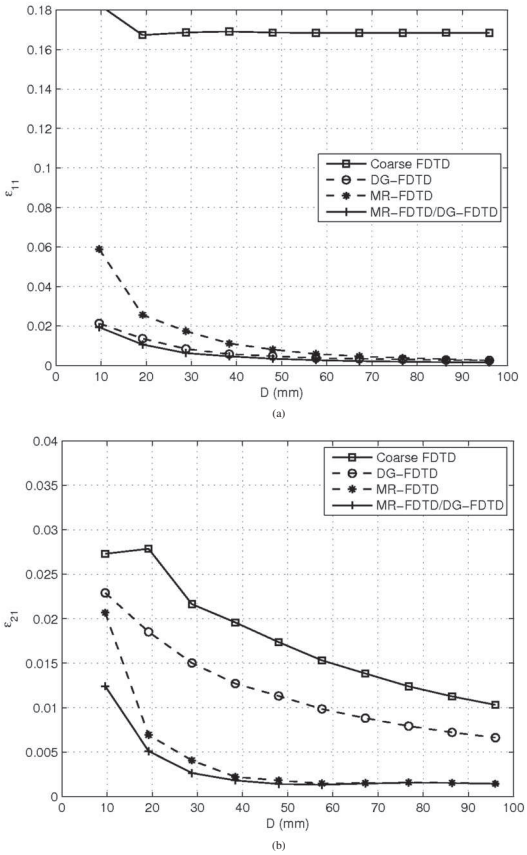

Fig. 9. Errors ϵ as a function of the simulation approach and the distance D between the antennas: (a) ϵ_{11}, (b) ϵ_{21}.

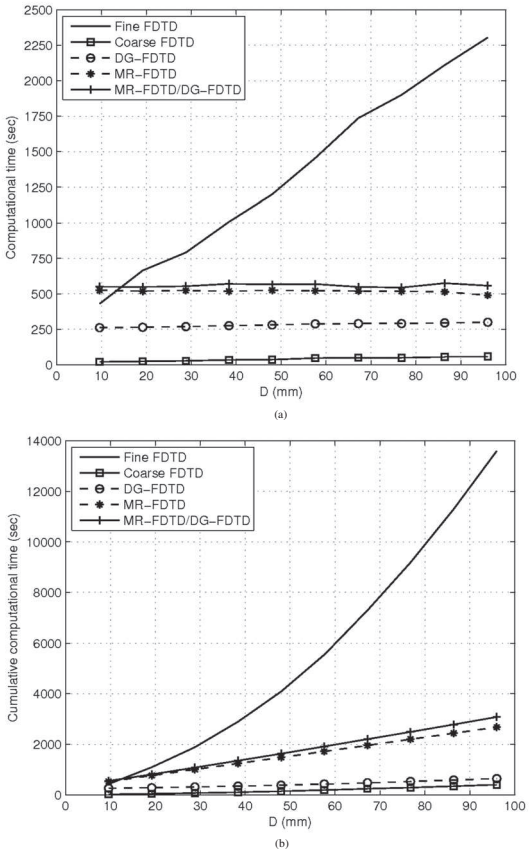

Fig. 10. (a) computational time, (b) cumulative computational time, as a function of the simulation approach and the distance D between the antennas.

	Reference FDTD	Coarse FDTD	DG-FDTD	Unilateral MR-FDTD	MR-FDTD/DG-FDTD
Sub-volume (a): Antenna 1	-	-	$_{,0}$=140	$_{,0}$=140	$_{,0}$=140
Sub-volume (b): Antenna 2	-	-	-	$_{,0}$=140	$_{,0}$=140
Volume (c): Antennas 1 and 2	$_{,0}$=140	$_{,0}$=35	$_{,0}$=35	-	$_{,0}$=35

Table 2. Different simulation approaches: FDTD volumes involved and their mesh densities.

tenna 2 for the MR-FDTD, and these two simulations for the MR-FDTD/DG-FDTD. Thus, the larger the number of configurations, the more competitive the multiresolution approaches.
Considering both accuracy and time criteria, the hybrid approach turns out to be the best trade-off to analyze the coupling between these antennas.

V. Conclusion

In this paper, two improvements of the dual-grid FDTD have been presented.
First of all, a correction procedure has been successfully applied to the DG-FDTD simulation of an integrated lens antenna. The far-field radiation patterns and the reflection parameter have been evaluated with a good accuracy. The correction procedure is particularly useful for the analysis of highly resonant structures that are not precisely described during the second step of the DG-FDTD. Although the correction procedure implies a third simulation, the computational speedup is still equal to 16.7.
Secondly, an hybrid solution has been proposed to the analysis of problems where the environment must be finely discretized. The MR-FDTD/DG-FDTD approach has been applied to study the coupling between two UWB antennas. Results have shown a reduction of the computational time for the hybrid approach while providing accurate results on the S parameters.

Acknowledgements

This work was supported by France Télécom Research & Development, contract no.46129586.

References

[1] Yee, K.S.: Numerical solution of initial boundary value problems involving Maxwell's equations in isotropic media. IEEE Trans. Antennas Propag. **AP14** (1966), 302-307.
[2] Sheen, D. et al.: Application of the three-dimensional finite-difference time-domain method to the analysis of planar microstrip circuits. IEEE Trans. Microw. Theory Tech. **38** (1990), 849-857.
[3] Krumpholz, M. et al.: MRTD: New time-domain schemes based on a multiresolution analysis. IEEE Trans. Microw. Theory Tech. **44** (1996), 555-571.
[4] Johnson, J.M. et al.: Multiple region FDTD (MR/FDTD) and its application to microwave analysis and modeling. 1996 IEEE MTT-S Int. Microwave Symp. Dig., San Fransisco, USA, 17-21 June 1996, 1475-1478.
[5] Laisné, A. et al.: A new multiresolution near-field to near-field transform suitable for multi-region FDTD schemes. 2001 IEEE MTT-S Int. Microwave Symp. Dig., Phoenix, USA, 20-25 May 2001, 893-896.
[6] Parfitt, A.J. et al.: Computation of aperture antenna mutual coupling using FDTD and Kirchhoff field transformation. Electron. Lett. **34** (1998), 1167-1168.
[7] Kunz, K.S. et al.: A technique for increasing the resolution of finite-difference time-domain solution of the Maxwell equation. IEEE Trans. Electromagn. Compat. **23** (1981), 419-422.
[8] Choi, D.H. et al.: A graded mesh FD-TD algorithm for eigenvalue problems. Proc. 17th European Microwave Conf. Dig., Rome, Italy, September 1987, 413-417.
[9] Zivanovic, S.S. et al.: A subgridding method for the time-domain finite-difference method to solve Maxwell's equations. IEEE Trans. Microw. Theory Tech. **39** (1991), 471-479.
[10] Chevalier, M.W. et al.: FDTD local grid with material traverse. IEEE Trans. Antennas Propag. **45** (1997), 411-421.
[11] Okoniewski, M. et al.: Three-dimensional subgridding algorithm for FDTD. IEEE Trans. Antennas Propag. **45** (1997), 422-429.
[12] Bérenger, J.P.: A Huygens subgridding for the FDTD method. IEEE Trans. Antennas Propag. **54** (2006), 3797-3804.
[13] Pascaud, R. et al.: Dual-grid finite-difference time-domain scheme for the fast simulation of surrounded antennas. IET Microw. Antennas Propag. **1** (2007), 700-706.
[14] Pascaud, R. et al.: Nouvelle méthode multirésolution en FDTD. 15èmes Jounées Nationales Micro-ondes, Toulouse, France, 23-25 May 2007.
[15] Pascaud, R. et al.: Une amélioration de la MR-FDTD basée sur son hybridation avec la DG-FDTD. 15èmes Jounées Nationales Micro-ondes, Toulouse, France, 23-25 May 2007.
[16] Bérenger, J.P.: A perfectly matched layer for the absorption of electromagnetic waves. Journal of Computational Physics **114** (1994), 185-200.
[17] Taflove, A. et al.: Computational Electrodynamics: The Finite-Difference Time-Domain Method (3rd Edition). Artech House, 2005.
[18] Balanis, C.A.: Antenna Theory: Analysis and Design (2nd Edition). John Wiley & Sons, Inc., 1997.

[19] Wu, X. et al.: Design and characterization of single- and multiple-beam mm-wave circularly polarized substrate lens antennas for wireless communications. IEEE Trans. Microw. Theory Tech. **49** (2001), 431-441.
[20] Godi, G. et al.: Design and optimization of three-dimensional integrated lens antennas with genetic algorithm. IEEE Trans. Antennas Propag. **55** (2007), 770-775.
[21] Godi, G. et al.: Performance of reduced size substrate lens antennas for millimeter-wave communications. IEEE Trans. Antennas Propag. **53** (2005), 1278-1286.
[22] Chantraine-Barès, B. et al.: Design of a compact millimeter-wave lens antenna for satellite communications in Q-band. Proc. 26th ESA Antenna Tech. Workshop on Satellite Antenna Modeling and Design Tools, ESTEC, Noordwijk, The Netherlands, 12-14 November 2003, 229-236.
[23] Gedney, S.D.: An anisotropic perfect matched layer-absorbing medium for the truncation of FDTD lattices. IEEE Trans. Antennas Propag. **44** (1996), 1630-1639.
[24] Wu, X.H. et al.: Optimization of planar diamond antenna for single-band and multiband UWB wireless communications. Microw. Opt. Technol. Lett. **42** (2004), 451-455.

Romain Pascaud was born in France in 1981. He received the Engineering degree from the National Institute of Applied Sciences (INSA), Rennes, France, in 2004. Since 2004, he has been working toward the Ph.D. degree in electronics at the Institute of Electronics and Telecommunications of Rennes (IETR), Rennes, France.

His research interests include numerical methods applied to the computer-aided design (CAD).

Raphaël Gillard obtained his PhD degree in Electronics from INSA of Rennes in 1992 (Subject: Modelling of Active Integrated Antennas Using the Method of Moment).

He first worked as a research engineer in IPSIS, France, developing a method of moment software for the simulation of millimetre wave circuits. He joined INSA in 1993 as an assistant Professor. He contributed to the development of an FDTD code and to the experimentation of wavelet-based fast solvers in both time and frequency domains. Since 2001, he has been a Professor in the Antenna and Microwave Group of the Electronics and Telecommunications Institute of Rennes (IETR). He has been in charge of the EM Modelling and Optimisation activity until 2006. He is now co-chairing the Antenna and Microwave Group. Since 2004, he has been leading the Software Benchmark Activity within the European Network of Excellence ACE (Antenna Center of Excellence).

Raphaël Gillard is member of the Scientific Committees of EuCAP and JNM (French National Microwave Conference), in charge of the Antenna and Propagation sub-committee, and co-chairman of the French URSI-B section. His actual research interests concern computational electromagnetics, dielectric resonator antennas and reflectarrays.

Gaël Godi was born in France in 1980. He received the electronics engineering degree and the M.S. degree in electronics from the National Institute of Applied Science (INSA), Rennes, France, in 2003. In 2006, he received the Ph.D. degree from the University of Rennes 1, France.

His research interests include the analysis and optimization of dielectric lens antennas for millimeter-wave applications.

Joe Wiart received the Engineering degree from the Ecole Nationale Supérieure des Télécommunications (ENST), Paris, France, in 1992, and the Ph.D. degree in physics from ENST and Pierre and Marie Curie University, Paris, in 1995.

In 1992, he joined the Centre National d'Etudes des Télécommunications (CNET), France Telecom, Issy-les-Moulineaux, and spent three years involved with propagation in microcellular environment. Since 1994, he has been involved with the interaction of radio waves with the human body and on medical electronic devices. He is currently the Head of a group that deals with these questions at France Telecom R&D (formerly CNET). His research interests include electromagnetic compatibility (EMC), bioelectromagnetics, antenna measurements, computational electromagnetics, statistics, and signal processing.

Dr. Wiart is a Senior Member of the Société de l'Electricité, de l'-Electronique et des Technologies de l'Information et de la Communication (SEE) since 1998, and the President of French Commission K of the Union Radio Scientifique Internationale (URSI) devoted to electromagnetism in biology and medicine. He was Vice Chairman of the COST 244 and is a Member of the Steering Committee of COST 281. He is the Chairman of the CENELEC Technical Committee 211 Working Group in charge of mobile and base-station standards.

Renaud Loison received the Engineering and Ph.D. degrees from the National Institute of Applied Sciences (INSA), Rennes, France, in 1996 and 2000, respectively.

In 2000, he joined the Institute of Electronics and Telecommunications of Rennes (IETR), Rennes, France, as an Associate Professor. His current research interests include numerical methods applied to the computer-aided design and optimization of microwave circuits and antennas.

Man-Faï Wong was born in Hong-Kong in 1965. He received the Engineering degree in electronics from "Ecole Nationale d'Electronique, d'Electrotechnique, d'Informatique et d'Hydraulique de Toulouse", Toulouse, France in 1990 and Ph.D. degree in electrical engineering from Paris 7 University in 1993.

Since 1990, he has been with the Centre National d'Etudes des Télécommunications (CNET), now France Telecom R&D, in the fields of applied electromagnetics for telecommunications systems. He has developed electromagnetic techniques and tools and has been involved in the analysis and design of microwave circuits and antennas. Since 1997, he has been working on the interactions of radiowaves with human bodies and the electromagnetic compatibility of wireless systems in France Telecom R&D.

His research interests include electromagnetic theory, bio-electromagnetics, computational electromagnetics, modeling techniques and signal processing techniques for solving field problems involved in wireless systems. He is vice-president of commission B of CNFRS/URSI.